Journal of Applied Sciences

ISSN 1812-5654

science alert

ANSInet
an open access publisher
http://ansinet.com

Journal of Applied Sciences 13 (10): 1716-1721, 2013
ISSN 1812-5654 / DOI: 10.3923/jas.2013.1716.1721

Deformation Performance at High Temperature and Processing Maps of 49 MnVS3

Yuanfang Chen, Hongbin Xu, Huade Jiang and Guohua Guan
School of Materials Science and Engineering, Chongqing university of technology, Chongqing, China

Abstract: The hot compression experiments were carried out on Gleeble-1500D thermal simulator system and the hot deformation performance of non-quenched and tempered steel 49MnVS3 between 950°C~1200°C with strain rate of 0.1~10 sec^{-1} were investigated by processing maps of dynamic material model. The deformation zone where dynamic recovery and dynamic recrystallization occurred is obtained according to true stress-strain curve. The variation law of strain rate sensitive factor m and power dissipation η is analyzed. Based on the analysis on m,η and instability criterion|Î, the instability zone with strain of 0.3 and 0.5 is analyzed by contrastive analysis method. It is found that the hot processing safety zone of this metal accords to each other. Taking the deformation parameters when dynamic recrystallization happened in hot processing safety zone as deformation conditions, the optimal processing safety zones of this alloy are determined to be 2~10 sec^{-1} for strain rate and 1150~1200°C for processing temperature.

Key words: Non-quenched and tempered steel, hot compression,strain rate sensitive factor, power dissipation efficiency, processing maps

INTRODUCTION

The application of non-quenched and non-tempered simplified production process and saved energy. By using non-quenched and tempered steel, hot deformation during heat treatment process and cracks during quenching process could be avoided and cutting performance of parts could also be enhanced to improve the quality of products and decrease environment pollution caused by heat treatment. Furthermore, due to the better comprehensive mechanic property and uniform microstructure of non-quenched and tempered steel after forging or rolling process without any subsequent quenched and tempered heat treatment, this method has been widely applied to forging industry. The keys to applications of non-quenched and tempered steel technology are reasonable selection a series of technological parameters, such as temperature during forging process (i.e. heating temperature, forging-ending temperature) and cooling speed after forging procedure (Chen *et al*., 2001; Tang *et al*., 2001). In this study, one pass hot compression experiments on 49MnVS3 non-quenched and tempered steel were carried out to study the stress-strain distribution of material on different deformation conditions. the deformation behavior of material at high temperature was investigated using hot processing maps which are based on Dynamic Material Model (DMM) to provide references to establish and optimize practical hot-process.

EXPERIMENT

Non-quenched and tempered steel 49MnVS3 was selected in our work, the main compositions are described as following: C: (0.44~0.52)%, Si :(0.15~0.6)%, Mn: (0.7~1.0)%, V: (0.08~0.15)%, S: (0.035~0.075)%, P≤0.035%, Cr≤0.3%. The samples used on Gleeble-1500D thermal simulator system for one pass isothermal hot-compression experiments derived from hot-rolled bars and were machined to cylindrical species with a size of Φ 10×12 mm. To decrease the friction between samples and indenters, tantalum sheets were placed on both ends of sample and compression deformation was 50% with and 1200°C, the deformation speed are 0.1, 1, 5 and 10 sec^{-1}, respectively. Before compressing process, species were heated to 1250°C with a heating rate of 10°C sec^{-1} with dwell time of 300 sec. In the end, samples were cooled down to individual deformation temperatures with a rate of 5°C sec^{-1}. After that, isothermal compression experiments were carried out with different strain rate. Ar gas was used to prevent species surface from oxidation during compression process. Water quenching method was used after compression process to preserve high temperature deformation structure.

RESULTS AND DISCASSION

Stress-strain curves: As shown in Fig. 1, flow stress increased quickly as increase of strain and tended to be

Corresponding Author: Yuanfang Chen, School of Materials Science and Engineering, Chongqing University of Technology, Chongqing, China

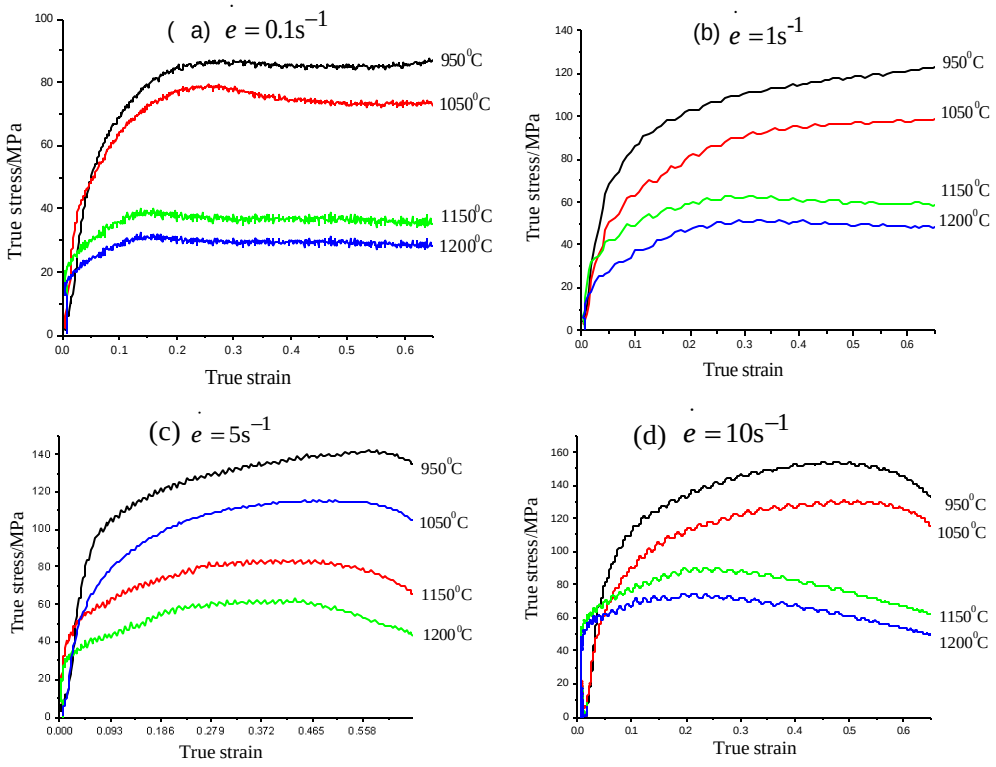

Fig. 1(a-d): Stress-strain curves of 49MnVS3 at different temperatures and different strain rates

stable or decreased after achieve to peak values. In initial stage of deformation, due to dislocation multiplication caused by plastic deformation, dislocation density increases and interaction among dislocations become stronger which result in increase of flow stress. Work hardening plays leading roll in this stage. Distortion energy resulted from dislocation stress field would become driving force to recrystallization after reaching a certain level. And dynamic recrystallization occurs. When the distortion energy in the metal could not reach critical energy which is necessary for dynamic recrystallization, dynamic recovery happens. When softening effect induced by dynamic recrystallization is balanced against work hardening, flow stress would remain a stable value. When softening effect is stronger than work hardening, the curve would show reduction tendency. At the same deformation temperature, flow stress increases as strain rate increases. However, flow stress decreases with the increase of deformation temperature. As observed in the curves, dynamic recovery phenomenon is shown clearly at respective temperature at strain rate of 0.1 sec^{-1}. Nevertheless, the obvious dynamic recrystallization is indicated at 1150 and 1200°C with high strain rate of 10 sec^{-1}.

Hot processing maps theory of DMM: DMM (Prasad and Rao, 2008; Prasad and Rao, 2005; Prasad *et al*., 1984; Ganesan *et al*., 2005; Meng *et al*.,2009) is established on basic fundamental theories such as continuum mechanics with large plastic deformation, physical system simulation and irreversible thermodynamics etc. The essential principle of this model can be described as following: during plastic deformation process, total energy P introduced from outside to workpiece, which is considered to a energy dissipation part, could be consumed in two fields: (1) Energy expended on plastic deformation. The most part is transferred into thermal energy, the other part is stored as crystal defect energy, which is expressed as G content, (2) The energy consumed by microstructure evolution during plastic deformation process. That would be name as J co-content . This procedure could be described using following mathematical expression:

$$P = \sigma\dot{\varepsilon} = G + J = \int_0^{\dot{\varepsilon}} \sigma d\dot{\varepsilon} + \int_0^{\sigma} \dot{\varepsilon} d\sigma \quad (1)$$

The ratios of two kinds of energy are determined by strain rate sensitive factor m at a certain strain:

$$m = \frac{dJ}{dG} = \frac{\dot{\varepsilon} d\sigma}{\sigma d\dot{\varepsilon}} = \frac{d\log\sigma}{d\log\dot{\varepsilon}} \quad (2)$$

At certain temperature and strain, the stress σ and strain rate ε loaded on workpiece would accord to the power law:

$$\sigma = K\dot{\varepsilon}^m \quad (3)$$

So, the J co-content can be expressed as:

$$J = \int_0^{\sigma} \dot{\varepsilon} d\sigma = \frac{m\sigma\dot{\varepsilon}}{m+1} \quad (4)$$

In this equation, the value range of m is between 0 and 1, when m = 1, material is in a ideal linear dissipation condition, dissipation covariant component J achieves maximum and:

$$J = J_{max} = \sigma\dot{\varepsilon}/2 \quad (5)$$

For non-linear dissipation, power dissipation efficiency η, which is a dimensionless constant, is introduced to characterize power dissipation of material. So:

$$\eta = \frac{J}{J_{max}} = \frac{2m}{m+1} \quad (6)$$

Power dissipation figure is use to present a relation of power dissipation efficiency with deformation temperature and strain rate.

Based on maximum principle of large-strain plastic deformation (Ziegler, 1983) deduced the criterion for flow instability of material:

$$\xi(\dot{\varepsilon}) = \frac{\partial\log\left(\frac{m}{m+1}\right)}{\partial\log\dot{\varepsilon}} + m < 0 \quad (7)$$

Here, the parameter:

$$\xi(\dot{\varepsilon})$$

is a function of deformation and strain rate, in power dissipation figure, the region where this parameter is minus is call flow instability region and this figure is flow instability figure. Therefore, processing map is a stacking chart of power dissipation graph and instability graph in a space with strain rate and deformation temperature.

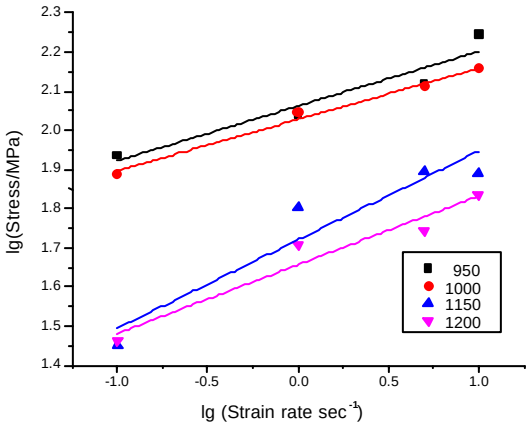

Fig. 2: Variation of flow stress (0.3 strain) with strain rate in log scale for 49MnVS3

Results and analysis: According to thermal compression simulation, the relations between 1 gσ and 1 gε with different strain were obtained and show obvious linear feature. Taking strain of 0.3 as an example, Fig. 2 indicates that 1 gσ and 1 gε show a stronger linear relation. It is suggests that the high temperature deformation of non-quenched and tempered steel 49MnVS3 accords to the module expressed by Eq. 3.

Influence of sensitive factorm: Figure 3 presents the complicated variation of m with different temperature and strain rate. It shows different tendency of strain rate sensitive factor with various strain. Such as, when ε = 0.3 and strain rate is between 1 and 5 sce^{-1}, m reduces first and then, increases as temperature increases, the minimum appears at 1150°C. When ε = 0.3, m also decreases first and then increases as temperature increases, but the minimum appears at 1000°C. When ε = 10, m increases first and then decreases, the maximum appears at 1150°C. When ε = 0.5 and strain rate is between 1 and 10 sec^{-1}, curve indicates a similar variation tendency with that when ε = 0.5. However, as ε = 0.1 m reduces first, then increases and decreases again in the end.

Because m is a function of power dissipation factor (η = 2 m/(1+m)), it is reasonable to use m to distinguish the position of instability region. Figure 4 presents the distribution of m depending on temperature and strain rate. In this figure, m is indicated by the values on isoplethic curves. Besides, in the gray region, m>0; in the dark region, m<0; in the dark gray region with oblique lines, m>0, but m is always relative smaller in this region. When strain is 0.3 min values appear in this figure (dark region). Usually, it is considered that some

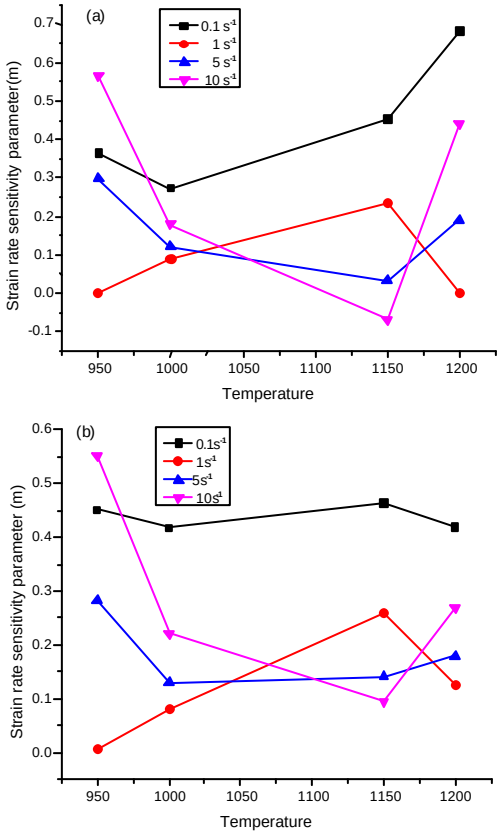

Fig. 3(a-b): Evolution of m as a function of temperature and strain rate for different strains (a) 0.3, (b) 0.5

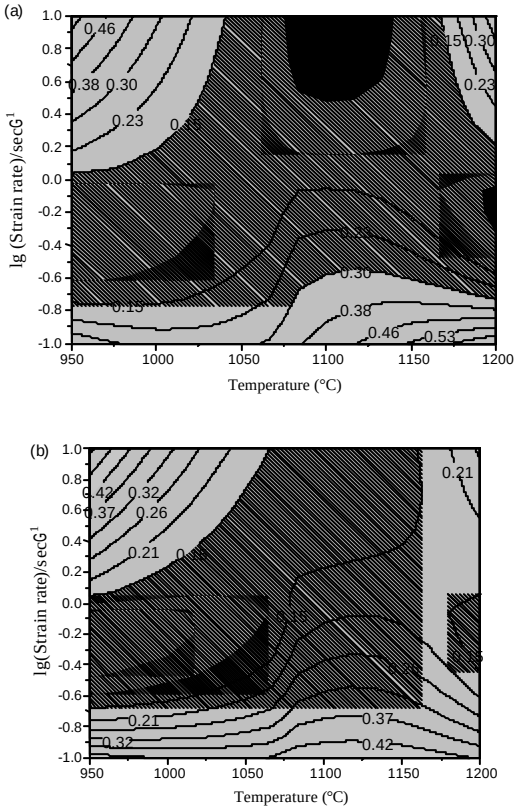

Fig. 4(a-b): Contour map for strain rate sensitivity parameter (m) for 49MnVS3 at a strain (a) 0.3, (b) 0.5

microdefects (i.e., dynamic aging, deformation twinning, microcrake and so on) (Zheng *et al*., 2011). Slipping deformation mechanism and low temperature twinning are the main reasons to result in the reduction of m. Consequently, it is necessary to select higher m as far as possible to avoid flow instability during forming process. (Zheng *et al*., 2011; Momeni and Dehghani, 2010) .

Power dissipation graph: Figure 5 is a power dissipation graph when strain is 0.3 and 0.5. In this figure, power dissipation coefficients in region I and II decrease rapidly. It is investigated that hot workability become worse remarkably and the flow instability probably exits in both regions. The dark part with strain of 0.3 shows negative η value. It is suggested that instability appear in material structure transformation (Kim *et al*., 2008; Tan *et al*., 2007). In addition, there are three peak areas in this figure and the positions where two peak areas with two strain lie on accord to each other. In peak area 1: Strain rate is between 4~10 sec^{-1}, temperature is in a range of 950-1050°C and the power dissipation coefficient is larger than 64%. In peak area 2: Strain rate is between 0.1~0.4 sec^{-1}, temperature is in a range of 1100-1200°C and the power dissipation coefficient is between 57 and 68%. In peak area 3, strain rate is between 4~10 sec^{-1}, temperature is in a range of 1150-1200 °C and the power dissipation coefficient is between 36 and 58%. The maximal power dissipation coefficient implies special microstructure and flow instability mechanism. Usually, high power dissipation area in power dissipation graph is defined as a optimum processing zone. However, since wedge-shaped cracks damage mechanism usually results in high power dissipation coefficient, it is necessary to determine this condition in combination of metallurgical structure of material after deformation (Bozzini and Cerri, 2002; Cavaliere, 2002; Gronostajski, 2002).

Hot processing maps and technology establishment: The gray region in Fig. 6a is the instability zone drafted based on the Eq. 7. The dark part presents the area with negative η. As mentioned above, this area is also called processing

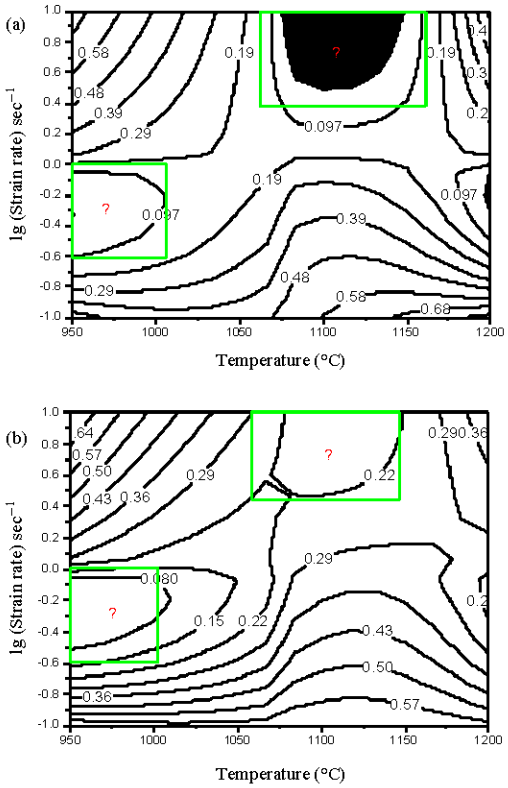

Fig. 5(a-b): Power dissipation graphs for 49MnVS3 obtained at strains of 0.3 and 0.5. The numbers against the contours represent efficiency of power dissipation in percent.The dark part in (a) Represent the flow instability and cracking

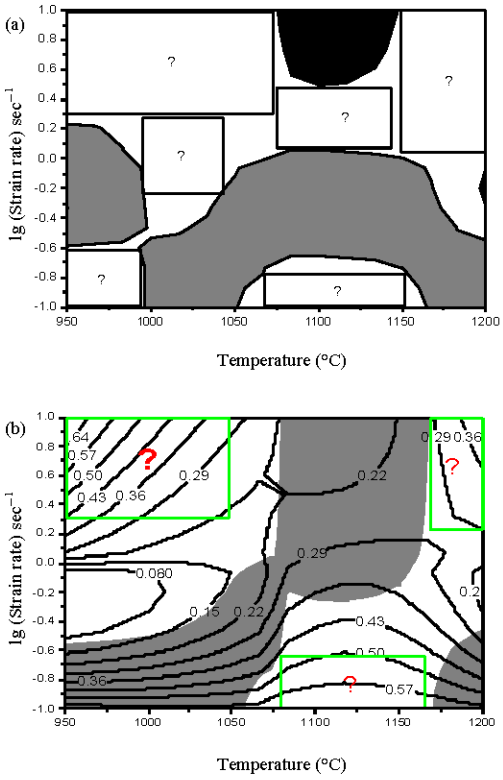

Fig. 6(a-b): Processing maps for 49MnVS3 obtained at strains of 0.3 and 0.5

instability zone. The rest region is divided into 6 zones which are marked by letters I, II, III, IV, V and VI, respectively. All these zones are processing non-instability zones including three peak areas I, IV, VI and other three zones in power dissipation graph. Combining distribution of m in Fig. 4, considering the zone with m larger than 0.15 as processing safety region, when strain is 0.3, it is suggested that the deformation conditions based on I, IV, VI could be used as fundament for selecting process.

Figure 6b is processing map with strain of 0.5. Comparing with the map with strain of 0.3, there are much differences in the shape of instability zone. However, taking the area whose m larger than 0.15 as an processing safety zone and combining this map with m distribution in Fig. 4b, the obtained locations of processing safety zones (I, II, III) agree with those with strain of 0.3 (I, IV, VI).

Hence, it can be seen, the processing safety zones based on three criteria m, η, ξ accords to each other.

Taking the processing map when stain = 0.5 (Fig. 6b) and according to the flow stress-strain curve in Fig. 1, it is suggested that dynamic recovery happened while ε is about 0.1 sec^{-1} and deformation temperature is between 1050 and 1150°C. That corresponds to the power dissipation coefficient of 57% in II of Fig. 6b. When strain rate is about 10 sec^{-1} and temperature is 950~1050°C, that would correspond to the maximal value of 64% in I of Fig. 6b. As shown as curves in Fig. 1d, there is no obvious dynamic recovery or recrystallization and instability is supposed to exist (Bozzini and Cerri, 2002; Cavaliere, 2002; Gronostajski, 2002). The maximal power dissipation coefficient is 36% in III zone of Fig. 6b. From Fig. 1d, when strain rate å is about 10 sec^{-1} and temperature is between 1150 and 1200°C, dynamic recrystallization occurs in metal. So, establishing process system should select dynamic recrystallization zone preferentially, owing to the good processing performance and easy-controlling of structure in this zone. Hence, the

best processing safety zone for non-quenched and tempered steel 49MnVS3 is in the III area (strain rate is 2~10 sec^{-1} and temperature is 1150~1200°C).

CONCLUSION

- Based on stress-strain curves obtained from experiment, it can be seen that dynamic recovery is shown obviously when strain rate is relative smaller (ε = 0.1 sec^{-1}). And dynamic recrystallization is obvious when strain rate is 10 sec^{-1}
- In this study, three criteria (m, η, ξ) are used with m distribution and processing map to distinguish processing safety zone for metal. Comparing processing safety zone with stain of 0.3 with that with strain of 0.5, it is found that both positions are similar
- When high temperature plastic deformation carried out on metal, there are three zones with higher power dissipation coefficient. The power dissipation coefficient of 36% is chosen as deformation parameter for dynamic recrystallization. The optimal processing safety zone for this metal is determined as strain rate is 2~10 sec^{-1} and temperature is between 1150~1200°C

ACKNOWLEDGMENT

This study is subsidized by the following project funding: The National Natural Science Fund (No: 51275548), the project of Chongqing scientific and technology (No: 2009AA3012-2) and Chongqing Municipal Education Commission Applied Basic Research Program of China (No: KJ120833).

REFERENCES

Bozzini, B. and E. Cerri, 2002. Numerical reliability of hot working processing maps. Mater. Sci. Eng. A, 328: 344-347.

Cavaliere, P., 2002. Hot and warm forming of 2618 aluminium alloy. J. Light Metals, 2: 247-252.

Chen, Y.B., W. Ma and K. Jin, 2001. Development on improving the strength and toughness of microalloyed steels. Mater. Mech. Eng., 25: 1-6.

Ganesan, G., K. Raghukandan, R. Karthikeyan and B.C. Pai, 2005. Development of processing map for 6061 Al/15% SiC_p through neural networks. J. Mater. Process. Technol., 166: 423-429.

Gronostajski, Z., 2002. The deformation processing map for control of microstructure in CuAl9.2Fe3 aluminium bronze. J. Mater. Process. Technol., 125-126: 119-124.

Kim, H.Y., H.C. Kwon, H.W. Lee, Y.T. Im, S.M. Byon and H.D. Park, 2008. Processing map approach for surface defect prediction in the hot bar rolling. J. Mater. Process. Technol., 205: 70-80.

Meng, G., B.L. Li, H.M. Li, H. Huang and Z. Nie, 2009. Hot deformation and processing maps of an Al-5.7 wt.%Mg alloy with erbium. Mater. Sci. Eng. A, 517: 132-137.

Momeni, A. and K. Dehghani, 2010. Characterization of hot deformation behavior of 410 martensitic stainless steel using constitutive equations and processing maps. Mater. Sci. Eng. A, 527: 5467-5473.

Prasad, Y.V.R.K. and K.P. Rao, 2005. Processing maps and rate controlling mechanisms of hot deformation of electrolytic tough pitch copper in the temperature range 300-950 °C. Mater. Sci. Eng. A, 391: 141-150.

Prasad, Y.V.R.K. and K.P. Rao, 2008. Processing maps for hot deformation of rolled AZ31 magnesium alloy plate: Anisotropy of hot workability. Mater. Sci. Eng. A, 487: 316-327.

Prasad, Y.V.R.K., H.L. Gegel, S.M. Doraivelu, J.C. Malas, J.T. Morgan, K.A. Lark and D.R. Barker, 1984. Modeling of dynamic material behavior in hot deformation: Forging of Ti-6242. Metallurgical Trans. A, 15: 1883-1892.

Tan, C.W., S.N. Xu, L. Wang, Z.Y. Chen, F.C. Wang and H,N. Cai, 2007. Effect of temperature on mechanical behavior of AZ31 magnesium alloy. Trans. Nonferrous Met. Soc. China, 17: 41-45.

Tang, X.M., J.Y. Chen, J.G. Zhao and H.Z. Ao, 2001. Development and application of non-quenched and tempered steels of bending and extending arms. Heat Treatment Metals, 1: 45-47.

Zheng, Q.G., Y. Wang and Y.W. Zhang, 2011. Construction for processing map based on DMM and identification for the stable hot-working parameters of Ti-6Al-2Zr-1Mo-1V alloy. J. Funct. Mater., 42: 2301-2306.

Ziegler, H., 1983. An Introduction to Thermomechanics. North-Holland Publishing Company, Amsterdam, New York, Oxford.